Available online at www.sciencedirect.com
SCIENCE DIRECT®
International Journal of Heat and Mass Transfer 47 (2004) 3993–4004
International Journal of HEAT and MASS TRANSFER
www.elsevier.com/locate/ijhmt

Mini- and micro-channels: influence of axial conduction in the walls

Gaël Maranzana, Isabelle Perry, Denis Maillet *

Laboratoire d'Energétique et de Mécanique Théorique et Appliquée, UMR 7563 CNRS, INPL, UHP Nancy 1, 2, avenue de la forêt de Haye, BP 160, 54504 Vandoeuvre–lès-Nancy cedex, France

Received 3 October 2003

Abstract

Heat transfer by conduction in the walls of mini–micro-channels can get a quite multidimensional character. The wall heat flux density, for small Reynolds numbers, can become strongly non-uniform: most of the flux is transferred to the fluid flow at the entrance of the mini–micro-channel. Two analytical models of channel between parallel plates are proposed. It is shown that inverting experimental measurements using a one-dimensional model, for small flow rates, may lead to an underestimation of heat transfer coefficients. Another conclusion is that axial conduction in the walls of a mini–micro counter-flow heat exchanger yields a loss of efficiency: an optimal wall conductivity that maximises this efficiency exists. A new non-dimensional number quantifying the part of axial conduction in walls is proposed.

1. Introduction

One particular characteristic of conductive heat transfer at mini–micro scales is its rather strongly multidimensional character. The lower the hydraulic diameter is, the more important the coupling between wall and bulk fluid temperatures becomes because the h transfer coefficient reaches large values. The consequence is that the axial conductive heat transfer in the wall cannot be neglected and that, the wall heat flux density cannot stay uniform: heat transfer mainly occurs at the entrance of mini–micro-channels. The term mini–micro-channel relates here to channels whose hydraulic diameter lies in the 10 μm to a few millimeters range, a scale where the double layer effects as well as the velocity slip condition can be neglected and where the Navier Stokes equations as well as the Fourier law are still valid. The axial conduction wall effect does not stem from the appearance of a new phenomenon but, as Herwig and Hausner [1] or Guo et al. [2] have noticed, of scaling effects with respect to a standard macro-analysis.

The experimental estimation of convective heat transfer h coefficients requires the use of a heat conduction model for the wall because direct measurements of temperature and wall heat flux at the interface between fluid and solid and direct local measurement of the bulk temperature of the fluid are very difficult to implement. Until now, the scientist community involved in these h measurements ([3–7] etc.) used to apply the model valid for most macro-channels—one-dimensional (perpendicular to the flow) heat conduction in the wall—to mini–micro-channels. So, the wall heat flux density is considered to be uniform along the channel [3–7]. The local temperature difference between the wall and the fluid is then calculated, either by choosing a linear variation for the bulk temperature of the fluid [5,7], or by considering an extrapolation of the parallel flow heat exchanger modelling and by choosing the logarithmic mean temperature difference [4]. Another assumption consists in considering this bulk temperature to be constant and equal to the inlet bulk temperature [3,6]. Recently, Herwig and Hausner [1] have shown that these assumptions are not always valid for mini–micro-channels. Not taking into account the non-uniformity of the

* Corresponding author. Tel.: +33-03-8359-5607/5606; fax: +33-03-8359-5531.
E-mail address: dmaillet@ensem.inpl-nancy.fr (D. Maillet).

0017-9310/$ - see front matter © 2004 Elsevier Ltd. All rights reserved.
doi:10.1016/j.ijheatmasstransfer.2004.04.016

Nomenclature

a	thermal diffusivity, $m^2 s^{-1}$
$\boldsymbol{A}$, $\boldsymbol{B}$, $\boldsymbol{C}$	quadrupole matrices
Bi	Biot number
c	specific heat, $J K^{-1} m^{-3}$
e	thickness, m
$\boldsymbol{G}$	wall-flow coupling matrix
h	convective heat transfer coefficient, $W m^{-2} K^{-1}$
L	length, m
M	"axial conduction" number
N	truncation order
No_q	norm of order q
NTU	number of transfer units
p	Laplace variable, s^{-1}
r	wall aspect ratio, e_s/L
T	temperature, K
T_0	initial temperature and bulk temperature at the inlet, K
V	fluid mean velocity, $m s^{-1}$
(x_i, z_i)	coordinate system linked to block i

Greek symbols

α_n	eigenvalue of order n
λ	thermal conductivity, $W m^{-1} K^{-1}$
φ	flux density, $W m^{-2}$
Φ	heat flux, W
ρ	mass density, $kg m^{-3}$
$\boldsymbol{\theta}$, $\boldsymbol{\phi}$	column vector of the harmonics of the Fourier transform of temperature and flux density
θ_n, ϕ_n	harmonics of order n of the Fourier transform of temperature and flux density
$\langle\cdot\rangle_x$	space average in x direction

Subscripts or superscripts

i	block number
f	fluid
s	solid
w	wall-flow interface
1D	one-dimensional model of conduction
exci	excitation

wall heat flux density (or the non-linear variation of the axial bulk temperature of the fluid), can lead to misinterpretations such as a variation of the Nusselt number with the Reynolds number for laminar flow in particular. We analyse this type of problem here and propose two analytical models of channel flow heat transfer between parallel plates. The potential inversion of measurements is considered, the axial conduction in the wall being taken into account. Several applications of these models explain the particular effects occurring in mini–micro-channel heat transfer. They are the consequences of axial conduction in the wall. For a counter-flow micro heat exchanger, axial conduction leads to a decrease in efficiency. So an optimal wall conductivity which maximises the heat exchanger efficiency exists.

2. Parameters of the problem

Let us consider the geometry shown in Fig. 1 which corresponds to a flow between two parallel plates: the channel of thickness e_f, of length L and width w is bounded by a wall of thickness e_s, of thermal conductivity λ_s, and a lower wall that corresponds to an adiabatic interface here. The heat excitation is associated with a uniform flux density φ_{exci} imposed on the upper face of the wall. The fluid flow is characterised by its mean velocity V and its bulk temperature $T^f(x)$. The coupling between the flow and the wall is done through a uniform heat transfer coefficient h.

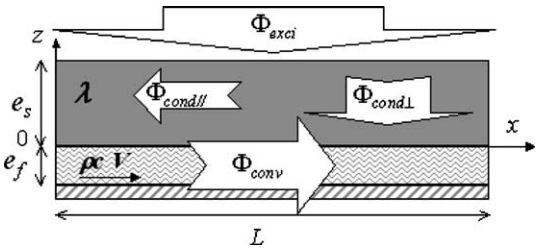

Fig. 1. Channel between two parallel plates.

The wall temperature T is governed by

$$\frac{\partial^2 T}{\partial x^2} + \frac{\partial^2 T}{\partial z^2} = 0, \tag{1}$$

$$\begin{aligned} &-\lambda_s \frac{\partial T}{\partial x}(x = 0, L; z) = 0, \\ &\lambda_s \frac{\partial T}{\partial z}(x, z = e_s) = \varphi_{exci} \geqslant 0, \end{aligned} \tag{2}$$

and the bulk temperature $T^f(x)$ of the flow is solution of

$$\rho c e_f V \frac{dT^f}{dx} = h(T(x, z = 0) - T^f(x)) = \lambda_s \frac{\partial T}{\partial z}(x, z = 0), \tag{3}$$

$$T^f(x = 0) = T_0^f. \tag{4}$$

So, the three natural non-dimensional parameters of the problem are

$$\mathrm{NTU}=\frac{hL}{\rho ce_{\mathrm{f}}V},\quad Bi=\frac{he_{\mathrm{s}}}{\lambda_{\mathrm{s}}},\quad r=\frac{e_{\mathrm{s}}}{L}, \tag{5}$$

that is to say a Biot number Bi based on the wall thickness, the wall size ratio r and a number of transfer units NTU. For physical interpretation reasons, the interesting phenomena being the axial conduction in the wall, we introduce an *axial conduction* number, see Fig. 1:

$$M=\frac{\Phi_{\mathrm{cond}//}}{\Phi_{\mathrm{conv}}}=\frac{\lambda_{\mathrm{s}}\frac{e_{\mathrm{s}}w}{L}}{\rho ce_{\mathrm{f}}wV}=\frac{r^2\,\mathrm{NTU}}{Bi}. \tag{6}$$

This non-dimensional number M allows to compare axial heat transfer by conduction in the wall and convective heat transfer in the flow. Φ_{conv} is the total convective heat flux (here equal to $\Phi_{\mathrm{exci}}=wL\varphi_{\mathrm{exci}}$) and $\Phi_{\mathrm{cond}//}$ is a heat flux characterising axial heat transfer in the wall:

$$\Phi_{\mathrm{conv}}=\rho ce_{\mathrm{f}}wV\Delta T^{\mathrm{f}}\quad\text{and}\quad\Phi_{\mathrm{cond}//}=\frac{\Delta T^{\mathrm{f}}}{R_{\mathrm{cond}//}}, \tag{7}$$

with

$$R_{\mathrm{cond}//}=\lambda_{\mathrm{s}}\frac{e_{\mathrm{s}}w}{L},\quad \Delta T^{\mathrm{f}}=T^{\mathrm{f}}(L)-T^{\mathrm{f}}(0). \tag{8}$$

Here $\Phi_{\mathrm{cond}//}$, which gives a rough estimation of the axial heat flux in the wall, is built assuming the transfer is one-dimensional (in the x-direction) through the same temperature difference ΔT^{f} than the one seen by the fluid. This number M is usually very low in the case of macro-channels (low $e_{\mathrm{s}}/e_{\mathrm{f}}$, large V and L) which implies that conductive heat transfer in walls is nearly one-dimensional and perpendicular to the fluid flow for these macroscopic cases. However this number can become quite large, when the size of the system decreases.

3. Reduced model for heat conduction in the wall

Let us consider now the problem shown in Fig. 1. A reduced model will be proposed for the solid and fluid temperature fields. This model is valid only when the Biot number Bi is very low. We consider the wall to behave as a thermal fin here, with a uniform temperature in its cross-section:

$$T^{\mathrm{s}}(x,z)=T^{\mathrm{s}}(x)\quad\text{assuming } Bi=\frac{he_{\mathrm{s}}}{\lambda_{\mathrm{s}}}\ll 1. \tag{9}$$

Integration of the heat equation (1) along the wall thickness yields

$$\frac{\mathrm{d}^2T^{\mathrm{s}}}{\mathrm{d}x^2}-\frac{h}{\lambda_{\mathrm{s}}e_{\mathrm{s}}}(T^{\mathrm{s}}-T^{\mathrm{f}})+\frac{\varphi_{\mathrm{exci}}}{\lambda_{\mathrm{s}}e_{\mathrm{s}}}=0, \tag{10}$$

where the excitation flux density φ_{exci} is assumed to be uniform here.

The energy balance (3) for the fluid flow yields

$$\frac{\mathrm{d}T^{\mathrm{f}}}{\mathrm{d}x}-\frac{h}{\rho ce_{\mathrm{f}}V}(T^{\mathrm{s}}-T^{\mathrm{f}})=0. \tag{11}$$

Integration of system (10) and (11) leads to the explicit solution of both temperatures as functions of M and NTU:

$$T^{\mathrm{f}}(x^*=x/L)=\mathrm{NTU}\,\frac{\varphi_{\mathrm{exci}}}{h}\left[x^*+M\left(1-\frac{\mathrm{e}^{\frac{\mathrm{NTU}}{2}(1-x^*)}\sinh(Px^*)+\mathrm{e}^{-\frac{\mathrm{NTU}}{2}x^*}\sinh(P(1-x^*))}{\sinh(P)}\right)\right], \tag{12}$$

$$T^{\mathrm{s}}(x^*)=\frac{\varphi_{\mathrm{exci}}}{h}\left(1+\mathrm{NTU}T\left\{x^*+M\left[1-\frac{\mathrm{e}^{-\frac{\mathrm{NTU}}{2}x^*}\left[\sinh(P(1-x^*))-\sqrt{1+4/M\,\mathrm{NTU}}\cosh(P(1-x^*))\right]}{2\sinh(P)}+\frac{\mathrm{e}^{\frac{\mathrm{NTU}}{2}(1-x)^*}\left[\sinh(Px^*)+\sqrt{1+4/M\,\mathrm{NTU}}\cosh(Px^*)\right]}{2\sinh(P)}\right]\right\}\right), \tag{13}$$

with

$$P=\sqrt{\left(\frac{\mathrm{NTU}}{2}\right)^2+\frac{\mathrm{NTU}}{M}}. \tag{14}$$

This solution is written as the sum of two terms, the first relative to the one-dimensional model of a thin wall and the second expressing the axial conduction in the wall. The M number naturally appears here as a factor of the second term. This very simple analytical model allows to estimate heat transfer coefficient using wall temperature measurements and taking axial heat conduction in the wall into account (see a simulation of inversion presented in Section 4.3).

4. Exact modeling of heat conduction in the wall

The preceding model is valid for very low Biot numbers constructed with the wall thickness. This assumption is not always valid for mini–micro-channels. Thus, the coming part is dedicated to the development of a more complete model that will be solved by the thermal quadrupole method [9,10].

4.1. The thermal quadrupole method

The thermal quadrupole method allows a quasi-analytical and rapid modeling of conductive transfer through geometries made of a stack of parallelepipedic

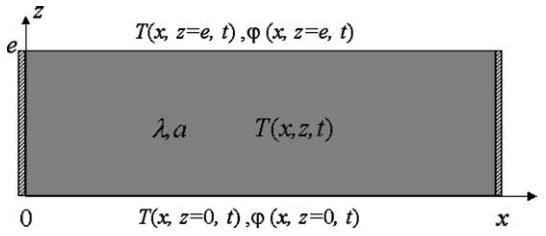

Fig. 2. Block whose lateral faces are insulated.

blocks. Let us consider a homogenous block in space whose lateral faces are insulated as shown in Fig. 2. In the two-dimension domain constituted by the block, the transient heat equation is written:

$$\begin{aligned} &\Delta T(x,z,t) = \frac{1}{a_s}\frac{\partial T(x,z,t)}{\partial t}, \\ &-\lambda_s \frac{\partial T}{\partial x}(x,z,t) = 0 \quad \text{for } x = 0 \text{ and } x = L, \\ &T(t=0) = T_0, \end{aligned} \tag{15}$$

where a_s and λ_s are the diffusivity and the conductivity of the material.

Applying a Fourier-cosinus transform of the x-coordinate and a Laplace transform in time allows to solve this system and to write the input–output relation relative to the block in the transformed space. The double transform is defined by

$$\theta_n(z,p) = \int_{x=0}^{L}\int_{t=0}^{\infty} T(x,z,t)\exp(-pt)\cos(\alpha_n x)\,\mathrm{d}t\,\mathrm{d}x, \tag{16}$$

$$\phi_n(z,p) = \int_{x=0}^{L}\int_{t=0}^{\infty} -\lambda\frac{\partial T}{\partial z}(x,z,t)\exp(-pt)\cos(\alpha_n x)\,\mathrm{d}t\,\mathrm{d}x, \tag{17}$$

where p is the Laplace variable, n the order of the considered harmonic and $\alpha_n = n\pi/L$ the eigenvalue of order n corresponding to the lateral dimension of the block. The input–output relation is written, using column spectrum vectors:

$$\begin{aligned} &\begin{bmatrix} \boldsymbol{\theta}(0,p) \\ \boldsymbol{\phi}(0,p) \end{bmatrix} = \begin{bmatrix} \boldsymbol{A}(p) & \boldsymbol{B}(p) \\ \boldsymbol{C}(p) & \boldsymbol{A}(p) \end{bmatrix} \begin{bmatrix} \boldsymbol{\theta}(e,p) \\ \boldsymbol{\phi}(e,p) \end{bmatrix}, \\ &A_n = \mathrm{ch}(\gamma_n e), \;\; B_n = 1/\lambda_s\gamma_n \mathrm{sh}(\gamma_n e), \\ &C_n = \lambda_s\gamma_n \mathrm{sh}(\gamma_n e), \;\; \gamma_n^2 = (n\pi/L)^2 + p/a_s, \end{aligned} \tag{18}$$

where the square diagonal matrices $\boldsymbol{A}$, $\boldsymbol{B}$ and $\boldsymbol{C}$ are transfer matrices and where $\boldsymbol{\theta}$ and $\boldsymbol{\phi}$ are the spectrum vectors of temperature and flux density truncated to keep N modes:

$$\boldsymbol{\theta} = (\,\theta_1 \quad \cdots \quad \theta_N\,)^{\mathrm{t}} \quad \text{and} \quad \boldsymbol{\phi} = (\,\phi_1 \quad \cdots \quad \phi_N\,)^{\mathrm{t}}. \tag{19}$$

The knowledge of two boundary conditions allows the calculation of the two other ones (temperature or flux in $z = 0$ or in $z = e$). This relationship (18) is exact and the only source of error is the necessary truncation of the different spectra. Temperature and flux density inside the block are calculated by dividing the block into several layers (each layer constituting one block). The return to the real space is then calculated through an inverse Fourier transformation:

$$\begin{aligned} &\overline{T}(x,z,p) = \sum_{n=0}^{N} \frac{\theta_n(z,p)}{No_n}\cos\left(\frac{n\pi}{L}x\right), \\ &No_0 = L, \;\; \underset{n\geqslant 1}{No_n} = \frac{L}{2}. \end{aligned} \tag{20}$$

This first inversion is followed by an inverse Laplace transform, which is numerically computed according to the Stefhest algorithm [11]. Let us remark that the case $p = 0$ corresponds to steady state conditions where Eq. (18) also stands for simple Fourier transforms of temperatures and heat flux densities.

4.2. Coupling transfer in the wall with a fluid flow of bulk temperature $T^f(x,t)$

Let us consider the geometry shown in Fig. 3, where a fluid flow in a channel of thickness e—constant mean velocity V, volumetric thermal capacitance ρc, bulk temperature $T^{\mathrm{f}}(x,t)$—is subjected to a wall heat flux $\varphi^{\mathrm{w}}(x,t)$ (from the wall to the fluid) at time $t = 0$. The lower face of the channel is insulated. The initial temperature of the system is assumed to be uniform and equal to the inlet temperature of the fluid. They are both noted T_0^{f}. This case is the same as above—Section 2—but the excitation is neither uniform nor steady and the wall is not considered yet. The equation governing the bulk temperature of the flow is

$$\varphi^{\mathrm{w}}(x,t) = \rho c e\left(\frac{\partial T^{\mathrm{f}}(x,t)}{\partial t} + V\frac{\partial T^{\mathrm{f}}(x,t)}{\partial x}\right). \tag{21}$$

Applying a Laplace transform in time—upper bar on the transformed quantities—and considering the relative heating $\Delta\overline{T}^{\mathrm{f}}(x,p) = \overline{T}^{\mathrm{f}}(x,p) - T_0^{\mathrm{f}}/p$, Eq. (21) becomes

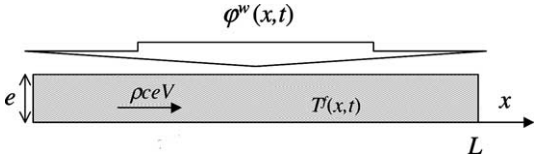

Fig. 3. Fluid flow subjected to a non-uniform wall heat flux density.

$$\bar{\varphi}^{\mathrm{w}}(x,p)=\rho ce_{\mathrm{f}}\left(p\Delta\overline{T}^{\mathrm{f}}(x,p)+V\frac{\partial\Delta\overline{T}^{\mathrm{f}}(x,p)}{\partial x}\right). \tag{22}$$

Integrating Eq. (22) by the method of variation of the constant yields:

$$\Delta\overline{T}^{\mathrm{f}}(x,p)=\frac{\int_0^x\bar{\varphi}^{\mathrm{w}}(x,p)\mathrm{e}^{\frac{p}{V}x}\,\mathrm{d}x}{\rho ceV}\mathrm{e}^{-\frac{p}{V}x}. \tag{23}$$

So, after replacing the flux density by its developed expression (according to (20)):

$$\Delta\overline{T}^{\mathrm{f}}(x,p)=\frac{\int_0^x\left(\sum_{q=0}^{N}\frac{\phi_q^{\mathrm{w}}(p)}{No_q}\cos(\alpha_q x)\right)\mathrm{e}^{\frac{p}{V}x}\,\mathrm{d}x}{\rho ceV}\mathrm{e}^{-\frac{p}{V}x}. \tag{24}$$

We still have to integrate Eq. (24) and to calculate the spectrum of $\Delta\overline{T}^{\mathrm{f}}(x,p)$ according to (16) using the same Fourier-cosinus transforms.

The final result is: for $n=0$ (fundamental of the spectrum)

$$\Delta\theta_0^{\mathrm{f}}=\frac{1}{\rho ceV}\left(\frac{p/VL-1+\mathrm{e}^{-\frac{p}{V}L}}{(p/V)^2}\frac{\phi_0^{\mathrm{w}}}{No_0}+\sum_{q=1}^{Q}\frac{\mathrm{e}^{-\frac{p}{V}L}-(-1)^q}{(p/V)^2+\alpha_q^2}\frac{\phi_q^{\mathrm{w}}}{No_q}\right), \tag{25}$$

and for $n\geqslant 1$ (harmonics of order $n\geqslant 1$)

$$\Delta\theta_n^{\mathrm{f}}=\frac{1}{\rho ceV}\left[\frac{\frac{p}{V}\frac{L}{2}}{(p/V)^2+\alpha_n^2}\frac{\phi_n^{\mathrm{w}}}{No_n}+\sum_{q=0}^{Q}\frac{(p/V)^2((-1)^n\mathrm{e}^{-\frac{p}{V}L}-1)}{((p/V)^2+\alpha_q^2)((p/V)^2+\alpha_n^2)}\frac{\phi_q^{\mathrm{w}}}{No_q}+\sum_{\substack{q=1\\q\neq n}}^{Q}\frac{\frac{q^2}{q^2-n^2}\left(1-(-1)^{n+q}\right)}{(p/V)^2+\alpha_q^2}\frac{\phi_q^{\mathrm{w}}}{No_q}\right]. \tag{26}$$

Eqs. (25) and (26) defines the coupling matrix $\boldsymbol{G}(p)$ between the wall flux density received by the fluid and the bulk temperature in the Laplace–Fourier domain. This matrix links the spectrum of the fluid heating to the spectrum of the wall heat flux density at the interface solid–fluid:

$$\Delta\boldsymbol{\theta}^{\mathrm{f}}(p)=\boldsymbol{G}(p)\boldsymbol{\phi}^{\mathrm{w}}(p). \tag{27}$$

Matrix $\boldsymbol{G}$ is full, which indicates a coupling between the different harmonics.

In steady state conditions ($p=0$), the expression of this matrix expression is rather simple:

$$\boldsymbol{G}_{n,q}=\frac{L}{2\rho ceV}\begin{pmatrix}1 & \cdots & \frac{4}{\pi^2}\frac{1-(-1)^q}{q^2} & \cdots\\ \vdots & 0 & \frac{4}{\pi^2}\frac{(-1)^{n+q}-1}{n^2-q^2} & \\ \frac{2}{\pi^2}\frac{(-1)^n-1}{n^2} & \frac{4}{\pi^2}\frac{(-1)^{n+q}-1}{n^2-q^2} & \ddots & \\ \vdots & & & 0\end{pmatrix}. \tag{28}$$

Moreover, the heating spectrum $\Delta\boldsymbol{\theta}^{\mathrm{f}}$ can be expressed as a function of the spectrum of the absolute temperature $\boldsymbol{\theta}^{\mathrm{f}}$:

$$\Delta\boldsymbol{\theta}^{\mathrm{f}}=\boldsymbol{\theta}^{\mathrm{f}}-\boldsymbol{\theta}_0^{\mathrm{f}}, \tag{29}$$

where $\boldsymbol{\theta}_0^{\mathrm{f}}$ is the spectrum of the inlet (and initial) temperature T_0^{f}:

$$\boldsymbol{\theta}_0^{\mathrm{f}}=\begin{pmatrix}T_0^{\mathrm{f}}L/p, & 0 & \cdots & 0\end{pmatrix}^{\mathrm{t}} \tag{30}$$

because this temperature T_0^{f} is a constant scalar.

To sum up, the preceding boundary condition is written in the formalism of the quadrupole method:

$$\begin{pmatrix}\boldsymbol{\theta}_0^{\mathrm{f}}\\ \boldsymbol{\phi}^{\mathrm{w}}\end{pmatrix}=\begin{pmatrix}\boldsymbol{I} & \boldsymbol{G}\\ \boldsymbol{0} & \boldsymbol{I}\end{pmatrix}\begin{pmatrix}\boldsymbol{\theta}^{\mathrm{f}}\\ \boldsymbol{\phi}^{\mathrm{w}}\end{pmatrix}, \tag{31}$$

where $\boldsymbol{I}$ is the identity matrix.

In the case where the convective heat transfer is characterised by a uniform heat transfer coefficient h: $-\varphi^{\mathrm{w}}(x,t)=h(T^{\mathrm{w}}(x,t)-T^{\mathrm{f}}(x,t))$ (the sign "−" comes from the fact that we consider an algebraic transfer from fluid to wall), that is to say: $\boldsymbol{\phi}^{\mathrm{w}}=h(\boldsymbol{\theta}^{\mathrm{f}}-\boldsymbol{\theta}^{\mathrm{w}})$.

The quadrupole relation equivalent to the boundary condition is thus

$$\begin{pmatrix}\boldsymbol{\theta}_0^{\mathrm{f}}\\ \boldsymbol{\phi}^{\mathrm{w}}\end{pmatrix}=\begin{pmatrix}\boldsymbol{I} & \boldsymbol{G}\\ \boldsymbol{0} & \boldsymbol{I}\end{pmatrix}\begin{pmatrix}\boldsymbol{I} & \boldsymbol{I}/h\\ \boldsymbol{0} & \boldsymbol{I}\end{pmatrix}\begin{pmatrix}\boldsymbol{\theta}^{\mathrm{w}}\\ \boldsymbol{\phi}^{\mathrm{w}}\end{pmatrix}(p). \tag{32}$$

4.2.1. Modeling a channel with its walls

Let us consider now a flow between two blocks numbered 0 and 1 as shown in Fig. 4. It is assumed that the fluid exchanges heat with the two blocks through the same uniform convective coefficient h. The equation governing the bulk temperature of the fluid is

$$\varphi^0(x_0,e_0,t)-\varphi^1(x_1,0,t)=\rho ce\left(\frac{\partial T^{\mathrm{f}}(x,t)}{\partial t}+V\frac{\partial T^{\mathrm{f}}(x,t)}{\partial x}\right). \tag{33}$$

Here wall heat flux densities φ^i ($i=1,2$) have their signs determined by the orientation of the z_i axis of the upper and lower blocks shown in Fig. 4.

In the double transformed domain, the relation between spectra, becomes—see (27):

$$\Delta\boldsymbol{\theta}^{\mathrm{f}}=\boldsymbol{G}(p)(\boldsymbol{\phi}^0(z_0=e_0,p)-\boldsymbol{\phi}^1(z_1=0,p)). \tag{34}$$

The definition of the h coefficient on the two walls can also been written using spectrum vectors:

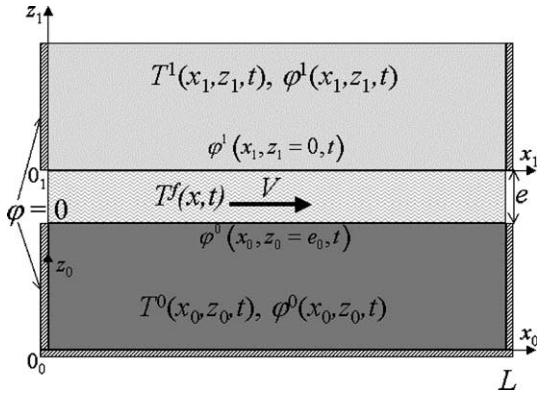

Fig. 4. Fluid flow between two parallel plates.

$$\boldsymbol{\phi}^0 = h(\boldsymbol{\theta}^0(z_0 = e_0, p) - \boldsymbol{\theta}^{\mathrm{f}}), \quad \boldsymbol{\phi}^1 = h(\boldsymbol{\theta}^{\mathrm{f}} - \boldsymbol{\theta}^1(z_1 = 0, p)). \tag{35}$$

The quadrupole matrix relative to the channel without its walls (transfer matrix of the flow) appears then naturally in the case where the inlet temperature T_0 is null ($\Delta\boldsymbol{\theta}^{\mathrm{f}} = \boldsymbol{\theta}^{\mathrm{f}}$). This matrix directly stems from Eqs. (34) and (35):

$$\begin{pmatrix} \boldsymbol{\theta}^0(z_0 = e_0) \\ \boldsymbol{\phi}^0(z_0 = e_0) \end{pmatrix} = \begin{pmatrix} \boldsymbol{I} & \boldsymbol{I}/h \\ 0 & \boldsymbol{I} \end{pmatrix} \begin{pmatrix} \boldsymbol{I} & 0 \\ \boldsymbol{G}^{-1} & \boldsymbol{I} \end{pmatrix} \begin{pmatrix} \boldsymbol{I} & \boldsymbol{I}/h \\ 0 & \boldsymbol{I} \end{pmatrix} \times \begin{pmatrix} \boldsymbol{\theta}^1(z_1 = 0) \\ \boldsymbol{\phi}^1(z_1 = 0) \end{pmatrix}. \tag{36}$$

The solution of the problem shown in Fig. 4, that incorporates conductive heat transfer in the walls with adiabatic lateral faces ($x = 0$ and $x = L$), is then

$$\begin{pmatrix} \boldsymbol{\theta}^0(z_0 = 0) \\ \boldsymbol{\phi}^0(z_0 = 0) \end{pmatrix} = \begin{pmatrix} \boldsymbol{A}^0 & \boldsymbol{B}^0 \\ \boldsymbol{C}^0 & \boldsymbol{A}^0 \end{pmatrix} \begin{pmatrix} \boldsymbol{I} & \boldsymbol{I}/h \\ 0 & \boldsymbol{I} \end{pmatrix} \begin{pmatrix} \boldsymbol{I} & 0 \\ \boldsymbol{G}^{-1} & \boldsymbol{I} \end{pmatrix} \times \begin{pmatrix} \boldsymbol{I} & \boldsymbol{I}/h \\ 0 & \boldsymbol{I} \end{pmatrix} \begin{pmatrix} \boldsymbol{A}^1 & \boldsymbol{B}^1 \\ \boldsymbol{C}^1 & \boldsymbol{A}^1 \end{pmatrix} \begin{pmatrix} \boldsymbol{\theta}^1(z_1 = e_1) \\ \boldsymbol{\phi}^1(z_1 = e_1) \end{pmatrix}, \tag{37}$$

where the solid block matrices $\boldsymbol{A}^i$, $\boldsymbol{B}^i$, $\boldsymbol{C}^i$ (for $i = 1, 2$) are defined in (18).

4.2.2. Numerical application for steady state conditions

A 3×10^4 W m^{-2} uniform excitation flux is imposed on the upper face of block 1 whose width (third dimension) is equal to unity. The lower face of block 0 is adiabatic. The two 10 mm long and 500 μm thick blocks are made out of silicon ($\lambda = 135$ W m^{-1} K^{-1}). Water flows in the 100 μm thick channel with a 5 cm s^{-1} velocity ($Re = 15.4$). For this application, one considers that there is no scale effect in the micro-channel and that the Nusselt number is uniform and equal to $Nu = 4.12$ which corresponds to an imposed flux boundary condition [8]. Thus $h = 25{,}950$ W m^{-2} K^{-1} for $\lambda_{\mathrm{f}} = 0.63$ W m^{-1} K^{-1} and the three parameters of the problem are: NTU = 12.4, $Bi = 0.10$ and $M = 0.32$. Simulated temperatures and flux densities are shown in Figs. 5 and 6. The bulk temperature variation is not linear at all. This is a consequence of large axial conduction effects. On this example, the bulk temperature reaches half of its maximal value after only about 1 mm of micro-channel. So half of the total excitation flux is communicated to the fluid flow on this first millimeter. The total flux received by block 0 is of course equal to zero, but this block helps to make the temperature more uniform along the x-coordinate: block 0 receives heat from the micro-channel in the downstream 9 mm to release it to the first millimeter upstream flow.

Fig. 7 shows the normalised bulk temperature variation $T_{\mathrm{f}}^* = (T_{\mathrm{f}}(x) - T_{\mathrm{f}}(0))/(T_{\mathrm{f}}(L) - T_{\mathrm{f}}(0))$ for several flow rates. We can remark that for this geometry axial conduction effects become negligible for M numbers lower than 0.01 ($Re = 500$). Of course, for a given geometry, the lower the Reynolds number the larger the axial conduction effects become: the fluid flow heats up in a sizeable way in the vicinity of the inlet section and consequently a large temperature gradient build up in the wall.

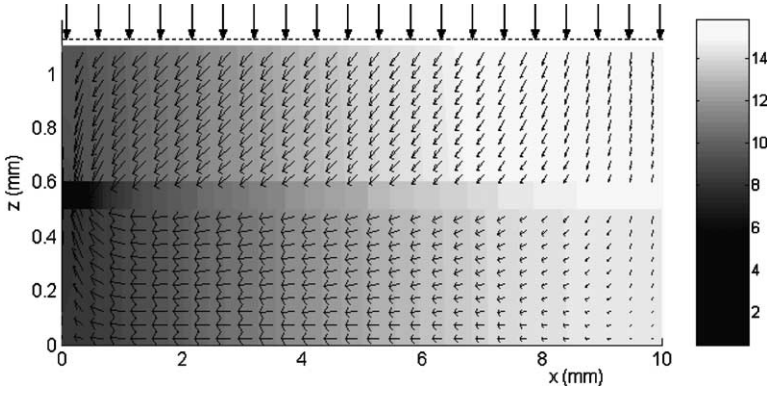

Fig. 5. Temperature (°C) and flux density in the system ($N = 100$).

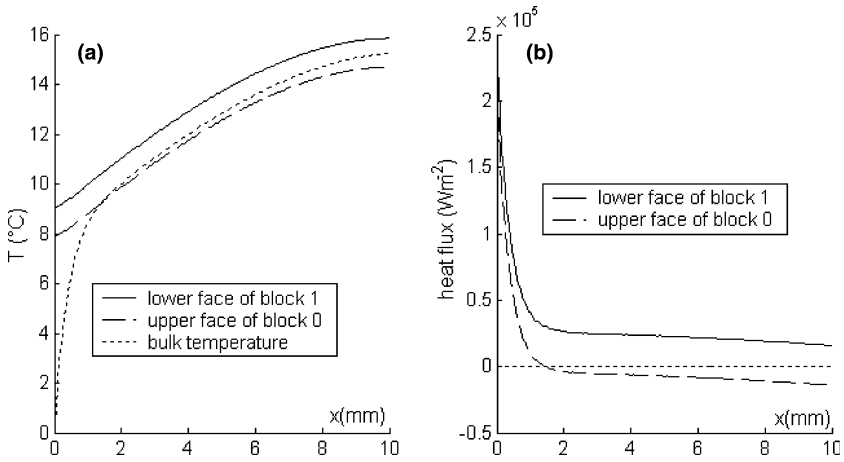

Fig. 6. (a) Interface temperature and (b) interface flux density.

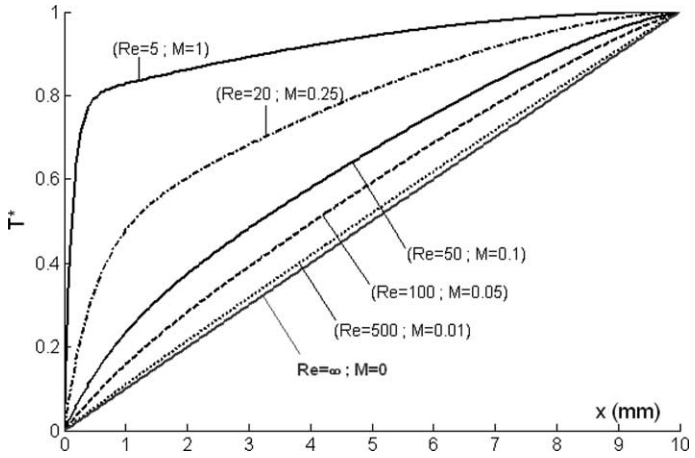

Fig. 7. Normalised bulk temperature as a function of x for several Reynold numbers.

4.2.3. Remarks on the assumption of a uniform h coefficient

The assumption of a uniform heat transfer coefficient seems to constitute here a restrictive hypothesis. The effects that we are trying to bring to the fore appear at the channel inlet, that is precisely at the location where heat transfer is not fully developed. The uniform h coefficient assumption is however necessary if the wall conduction effects have to be studied in a simple way. The same assumption is also a prerequisite in the model that will be used for estimating experimentally the local heat transfer coefficient, see Section 4.3. The only way of testing this assumption is to use a more sophisticated (less reduced) model by solving the conjugated transfer between wall and fluid without any transfer coefficient: the convection–diffusion equation can be solved in the fluid layer in laminar regime, with the calculation of a two-dimensional temperature distribution in the fluid, by the quadrupole method, see [12]. It is thus possible to derive the true local h coefficient by a calculation of the wall temperature and heat flux density, as well as the fluid bulk temperature calculated through an integration in the thickness of the fluid flow.

The same micro-channel as the one studied above ($e_1 = e_0 = 400$ μm; $e_f = 100$ μm; $L = 10$ mm), but with a symmetrical imposed flux onto faces $z_0 = 0$ and $z_1 = e_1$, with the same input data as above ($Re = 15$), is shown in Fig. 8. The bulk flow and interface wall temperatures are calculated with the two models, reduced model given by Eq. (37) and detailed model [12]. It is shown in this example that the error caused by the reduced model (uniform h assumption) is quite low when compared with the error caused by the use of a one-dimensional heat conduction hypothesis in the wall (that yields a

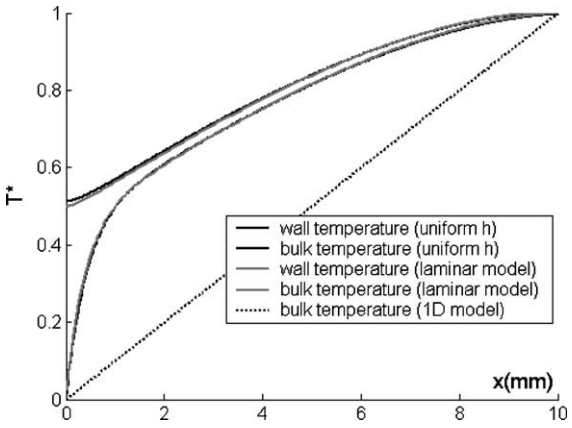

Fig. 8. Comparison between the reduced model (uniform h) and the exact model (laminar hydrodynamically developed model with 2D temperature field in the fluid).

linear variation of the bulk temperature of the fluid flow). The effect of axial conduction in the wall is much larger than the non-uniform h effect.

4.3. Simulating the estimation of a heat transfer coefficient

Scaling effects concerning heat transfer in mini–micro-devices are not clearly established. Often special effects are proposed to explain unexpected experimental results, great care has to be paid for inversion of the temperature measurements. We have recalled in Section 1 that a common assumption often made [3–7] is to consider the wall flux density uniform along the channels. However, according to Figs. 6 and 7, this wall flux density is far from staying uniform and the bulk temperature of the fluid does not vary linearly. This effect is especially important when the M number is large. Thus, one-dimensional models do not fit well for inverting measurements when the Reynolds number is low.

The preceding analytical model can allow to estimate a convective heat transfer coefficient starting from a non-intrusive temperature measurement (infrared thermography for example) on the external face of the channel. Here, a simulation of an experiment has been implemented for the preceding example of micro-channel. The simulated temperature on the upper face of block 1 ($z = e_1$) is sampled over 320 pixels, which represents the size of the array of an infrared camera detector. Then a Gaussian noise with zero mean and a 0.1 K standard deviation is added to simulate the experimental temperature. This experimental temperature field and the preceding model allows the estimation of the mean heat transfer coefficient h through a least square method. The corresponding simulated estimation of the convective coefficient is equal to 25,905 $\mathrm{W\,m^{-1}\,K^{-2}}$ (for an exact value used in the direct simulation of 25,950 $\mathrm{W\,m^{-1}\,K^{-2}}$). The relative error is thus lower than 2‰. By comparison the one-dimensional model assuming that the bulk temperature is linear, yields a mean convective heat transfer coefficient:

$$h_{1D} = \varphi_{1D} \Big/ \Big[\langle T(z_1 = 0) \rangle_{x_1} - (T^f(x = L) + T^f(x = 0))/2 \Big], \tag{38}$$

$$h_{1D} = 6100\ \mathrm{W\,m^{-2}\,K^{-1}} \quad (\neq 25,950\ \mathrm{W\,m^{-2}\,K^{-1}}). \tag{39}$$

This calculation leads to an underestimation of the convective coefficient, the error being very high here because the M number is not small ($M = 0.32$). This can explain the dependence of the Nusselt number on the Reynolds number noticed in most of the preceding experimental works in the case of laminar flows. Fig. 9

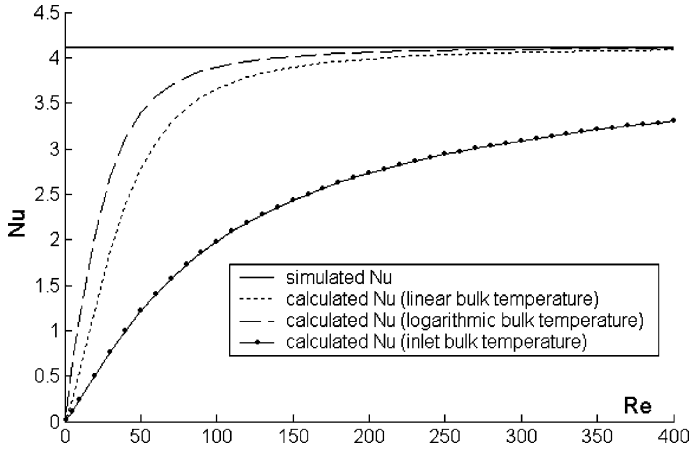

Fig. 9. Simulated and estimated Nusselt numbers using the 1D-models (1–3) for inversion.

shows estimated Nusselt numbers as a function of Reynolds numbers for the preceding geometry and the two one-dimensional conduction models (linear and constant bulk temperature). The preceding works have produced results that are clearly artefacts: inversions made with non pertinent models yield an apparent increase of the Nusselt number with the Reynolds number as well as an underestimation of this number. One can notice that the thermal quadrupole method is able to allow an estimation of the first harmonics of a non-uniform convective heat transfer coefficient $h(x)$ [10,13].

4.4. Modelling a parallel plate counter-flow heat exchanger

Let us consider now a counter-flow heat exchanger between parallel plates whose basic cell is shown in Fig. 10. The hot fluid of volumetric capacitance ρc_{hot} flows with the mean velocity V_{hot}. Its temperature is called T hot. The cold fluid of volumetric capacitance ρc_{cold} flows with the mean velocity V_{cold}. Its temperature is called T_{cold}. The preceding method allows to write in steady state conditions (see Appendix A):

$$\begin{pmatrix} \boldsymbol{\theta}^0_{\text{hot}} \\ \boldsymbol{\phi}_{\text{hot}} \end{pmatrix} = \begin{pmatrix} \boldsymbol{I} & \boldsymbol{G}_{\text{hot}} \\ 0 & \boldsymbol{I} \end{pmatrix} \begin{pmatrix} \boldsymbol{I} & \boldsymbol{I}/h_{\text{hot}} \\ 0 & \boldsymbol{I} \end{pmatrix} \begin{pmatrix} \boldsymbol{A} & \boldsymbol{B} \\ \boldsymbol{C} & \boldsymbol{A} \end{pmatrix} \times \begin{pmatrix} \boldsymbol{I} & \boldsymbol{I}/h_{\text{cold}} \\ 0 & \boldsymbol{I} \end{pmatrix} \begin{pmatrix} \boldsymbol{I} & \boldsymbol{G}_{\text{cold}} \\ 0 & \boldsymbol{I} \end{pmatrix} \begin{pmatrix} \boldsymbol{\theta}^0_{\text{cold}} \\ \boldsymbol{\phi}_{\text{cold}} \end{pmatrix}, \quad (40)$$

where $\boldsymbol{\theta}^0_{\text{hot}}$ and $\boldsymbol{\theta}^0_{\text{cold}}$ are the inlet temperatures spectra of the hot and cold flows.

According to Eq. (16), in steady state conditions (no Laplace transform):

$$\begin{aligned} \boldsymbol{\theta}^0_{\text{hot}} &= (\, T^0_{\text{hot}} L, \quad 0 \quad \cdots \quad 0\,)^{\text{t}} \quad \text{and} \\ \boldsymbol{\theta}^0_{\text{cold}} &= (\, T^0_{\text{cold}} L, \quad 0 \quad \cdots \quad 0\,)^{\text{t}}, \end{aligned} \quad (41)$$

where $\boldsymbol{\phi}_{\text{hot}}$ and $\boldsymbol{\phi}_{\text{cold}}$ are the wall flux density spectra (Fourier-cosine transforms) at the interface between the wall and the fluid flows. Solving the two-unknown two-equation system (40) yields the wall flux densities for the hot and the cold flows. Then, a direct calculation gives the fields of temperature and flux density in the wall.

4.4.1. Numerical application

Let us consider the case of a micro heat exchanger made of two silicon parallel plates of thickness $e_s = 500$ μm and of length $L = 10$ mm. The thickness of micro-channels is noted $e_f = 100$ μm. The hot fluid inlet temperature is equal to 60 °C, and the cold fluid to 10 °C. For this hydrodynamically developed laminar flow, the Nusselt number is assumed to be uniform and equal to $Nu = 4.12$, so $h = 25{,}950\ \text{W m}^{-2}\,\text{K}^{-1}$ (for $\lambda_f = 0.63\ \text{W m}^{-1}\,\text{K}^{-1}$). The volumetric capacitance of the water is also assumed to be constant: $\rho c = 4.18 \times 10^6\ \text{JK}^{-1}\,\text{m}^{-3}$ and the mean velocity of the two flows is equal to $V = 5\ \text{cm s}^{-1}$. So, the parameters of the problem are the same as for the preceding example: NTU = 12.4, $Bi = 0.10$ and $M = 0.32$.

Hundred harmonics are kept ($N = 100$). The temperature and flux density fields are shown in Fig. 11. We can remark on this example that the axial component of the flux density along the flow direction is very important. Conductive heat transfer in the walls of this micro-exchanger is strongly multidimensional here. Transfer occurs mainly near the inlet of each micro-channels. This effect is clearly shown in Fig. 12 which gives the variation of both fluid temperature and wall heat flux densities in the x-direction.

We can compare these results with the simpler one-dimensional heat exchanger model for which

$$T_{\text{hot}}(x) = \frac{\Delta T^0}{1/\text{NTU}_{\text{1D}} + 1}\left(\frac{x}{L} - 1\right) + T^0_{\text{hot}}, \quad (42)$$

$$T_{\text{cold}}(x) = \frac{\Delta T^0}{1/\text{NTU}_{\text{1D}} + 1}\frac{x}{L} + T^0_{\text{cold}}, \quad (43)$$

$$\text{NTU}_{\text{1D}} = \frac{L \Big/ \left(\frac{1}{h_{\text{hot}}} + \frac{1}{h_{\text{cold}}} + \frac{e_s}{\lambda}\right)}{\rho c e_f V}, \qquad \Delta T^0 = T^0_{\text{hot}} - T^0_{\text{cold}}. \quad (44)$$

For this particular case (same fluid, same flow rate) the two fluids temperature distributions are linear and not exponential. Fig. 13 allows the comparison of the two models, for the preceding example. The 1D-model overestimates heat transfer because it does not take into account the conduction thermal conductance in the axial

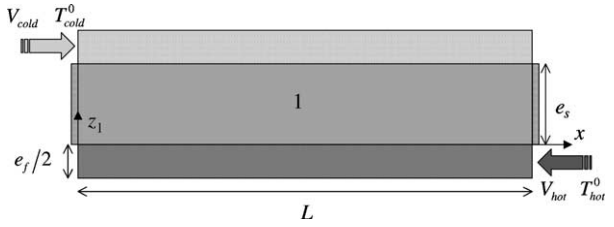

Fig. 10. Basic cell of a counter-flow heat exchanger with parallel plates.

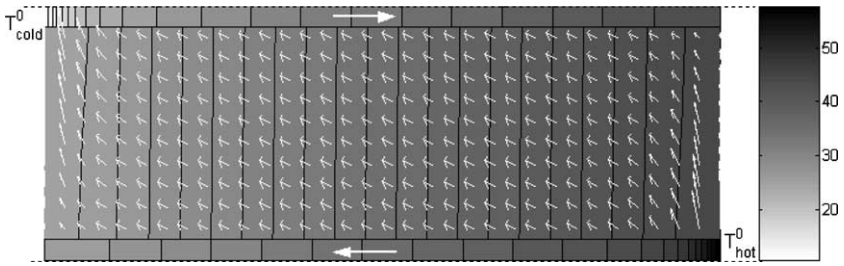

Fig. 11. Temperature and flux density fields in the basic cell.

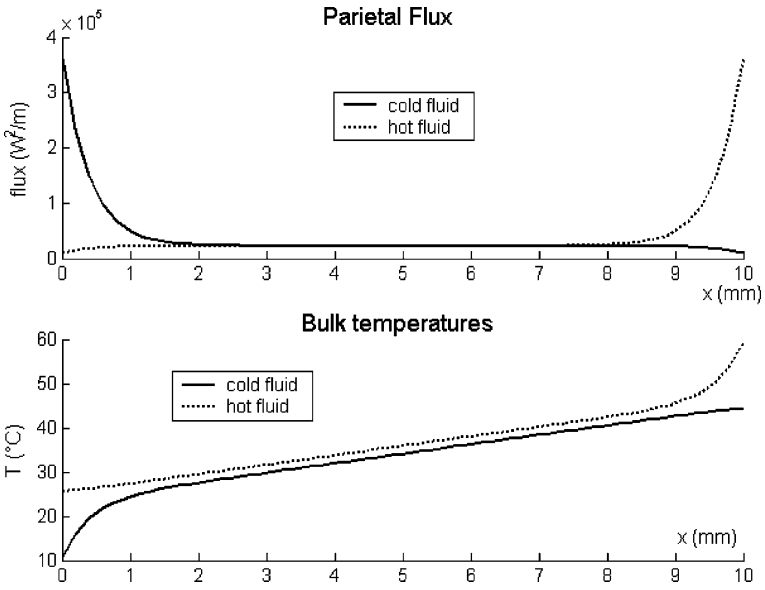

Fig. 12. Wall fluxes and fluids bulk temperatures.

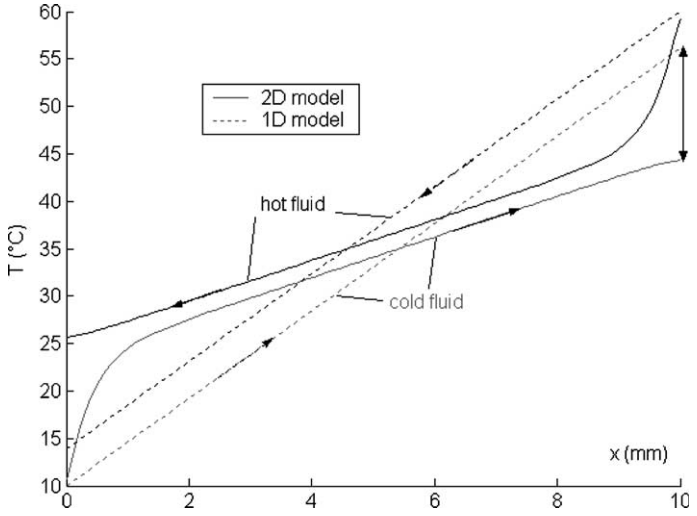

Fig. 13. Bulk temperatures—comparison between the 1D and 2D models.

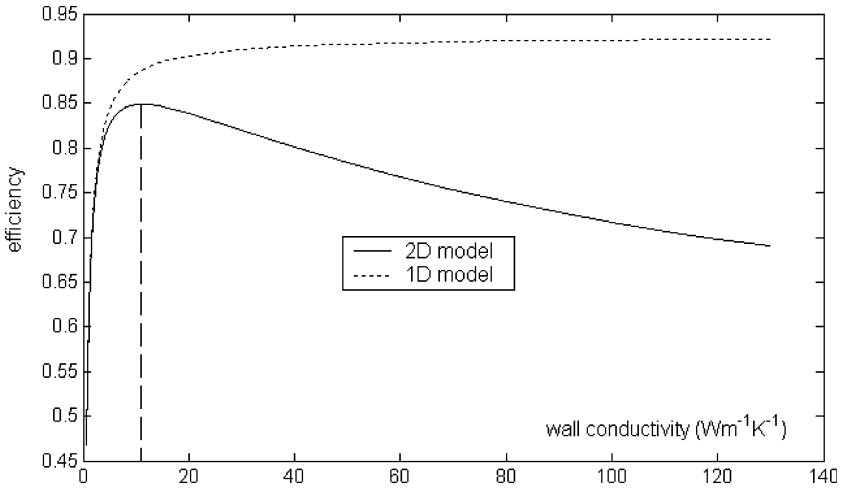

Fig. 14. Exchanger efficiency as a function of the wall conductivity.

direction. Moreover this axial conduction turns the counter-flow exchanger into a mixer (a system where the outlet temperatures of both fluids tend to be equal). The consequence of axial conduction is a lowering of the exchanger efficiency e:

$$e = \frac{T_{\text{cold}}(x = L) - T^0_{\text{cold}}}{T^0_{\text{hot}} - T^0_{\text{cold}}}.$$

So, it is clear that an optimal conductivity should exist for the wall [14]: this optimal conductivity must lower axial conductive transfer without penalizing too much conductive transfer in the thickness direction. The exchanger with the highest performance is not the one made out of the most conductive material. This optimal conductivity can be obtained very quickly by this model which is very efficient in terms of processing time, see Fig. 14. For this example, the optimal conductivity is equal to 11.2 $\mathrm{W\,m^{-1}\,K^{-1}}$. Here, a stainless heat exchanger will be more efficient than a copper one and the gain can reach 20%.

5. Conclusion

Modeling heat transfer in mini–micro-devices requires taking axial conduction in the walls into account. This phenomenon which is generally neglected in the standard macro-analysis stems from the small size of the systems. Disregarding this effect can lead to very large bias in the experimental estimation of heat transfer coefficients, especially for small Reynolds numbers. A new non-dimensional number M quantifying the relative part of conductive axial heat transfer in walls has been introduced. This number appears explicitly in the analytical solution corresponding to a fin assumption for the wall. Even if other non-dimensional numbers (Bi and NTU) and boundary conditions have an effect on axial conduction too, we have noticed that in the simulation of most cases that were studied, axial conduction can be neglected as soon as the M number gets lower than 10^{-2}. Two analytical models of heat transfer in channel flow between parallel plates are proposed and allow the application of an inverse method in order to estimate convective heat transfer coefficients. Axial conduction in the walls has to be considered too for designing mini–micro counter-flow heat exchangers: there exists an optimal conductivity for the wall which maximises the exchanger efficiency.

Appendix A

For the same reason as in Section 4.2, for the cold fluid flows in the x-increasing direction:

$$\begin{pmatrix} \boldsymbol{\theta} \\ \boldsymbol{\phi} \end{pmatrix}(z_1 = e_s) = \begin{pmatrix} \boldsymbol{I} & \boldsymbol{I}/h_{\text{cold}} \\ 0 & \boldsymbol{I} \end{pmatrix} \begin{pmatrix} \boldsymbol{I} & \boldsymbol{G}_{\text{cold}} \\ 0 & \boldsymbol{I} \end{pmatrix} \begin{pmatrix} \boldsymbol{\theta}^0_{\text{cold}} \\ \boldsymbol{\phi}_{\text{cold}} \end{pmatrix}. \tag{A.1}$$

Matrix $\boldsymbol{G}_{\text{cold}}$ is defined under steady state conditions by (28).

The hot fluid flows going in the x-decreasing direction, the coupling matrix $\boldsymbol{G}$ is slightly modified:

$$\begin{pmatrix} \boldsymbol{\theta}^0_{\text{hot}} \\ \boldsymbol{\phi}_{\text{hot}} \end{pmatrix} = \begin{pmatrix} \boldsymbol{I} & \boldsymbol{G}_{\text{hot}} \\ 0 & \boldsymbol{I} \end{pmatrix} \begin{pmatrix} \boldsymbol{I} & \boldsymbol{I}/h_{\text{hot}} \\ 0 & \boldsymbol{I} \end{pmatrix} \begin{pmatrix} \boldsymbol{\theta} \\ \boldsymbol{\phi} \end{pmatrix}(z_1 = 0), \tag{A.2}$$

with

$$G_{\text{hot}} = \frac{L}{2\rho c e_{\text{f}} V} \begin{pmatrix} 1 & \cdots & -\frac{4}{\pi^2}\frac{1-(-1)^q}{q^2} & \cdots \\ \vdots & 0 & -\frac{4}{\pi^2}\frac{(-1)^{n+q}-1}{n^2-q^2} & \\ -\frac{2}{\pi^2}\frac{(-1)^n-1}{n^2} & -\frac{4}{\pi^2}\frac{(-1)^{n+q}-1}{n^2-q^2} & \ddots & \\ \vdots & & & 0 \end{pmatrix}. \tag{A.3}$$

The transfer equation between the $z_1 = 0$ and $z_1 = e_s$ interfaces is written in accordance with (18):

$$\begin{pmatrix} \boldsymbol{\theta} \\ \boldsymbol{\phi} \end{pmatrix}(z_1 = 0) = \begin{pmatrix} \boldsymbol{A} & \boldsymbol{B} \\ \boldsymbol{C} & \boldsymbol{A} \end{pmatrix} \begin{pmatrix} \boldsymbol{\theta} \\ \boldsymbol{\phi} \end{pmatrix}(z_1 = e_{\text{s}}). \tag{A.4}$$

Finally the input–output equation of the entire system is found by combining Eqs. (A.1)–(A.4):

$$\begin{pmatrix} \boldsymbol{\theta}^0_{\text{hot}} \\ \boldsymbol{\phi}_{\text{hot}} \end{pmatrix} = \begin{pmatrix} \boldsymbol{I} & \boldsymbol{G}_{\text{hot}} \\ 0 & \boldsymbol{I} \end{pmatrix} \begin{pmatrix} \boldsymbol{I} & \boldsymbol{I}/h_{\text{hot}} \\ 0 & \boldsymbol{I} \end{pmatrix} \begin{pmatrix} \boldsymbol{A} & \boldsymbol{B} \\ \boldsymbol{C} & \boldsymbol{A} \end{pmatrix} \times \begin{pmatrix} \boldsymbol{I} & \boldsymbol{I}/h_{\text{cold}} \\ 0 & \boldsymbol{I} \end{pmatrix} \begin{pmatrix} \boldsymbol{I} & \boldsymbol{G}_{\text{cold}} \\ 0 & \boldsymbol{I} \end{pmatrix} \begin{pmatrix} \boldsymbol{\theta}^0_{\text{cold}} \\ \boldsymbol{\phi}_{\text{cold}} \end{pmatrix}. \tag{A.5}$$

References

[1] H. Herwig, O. Hausner, Critical view on "new results in micro-fluid mechanics": an example, Int. J. Heat Mass Transfer 46 (2003) 935–937.

[2] Z.Y. Guo, Z.X. Li, Size effect on microscale single-phase flow and heat transfer, Int. J. Heat Mass Transfer 46 (2003) 149–159.

[3] B. Wang, X. Peng, Experimental investigation on liquid forced-convection heat transfer trough microchannels, Int. J. Heat Mass Transfer 37 (1994) 73–82.

[4] X. Peng, G. Peterson, Convective heat transfer and flow friction for water flow in microchannels structures, Int. J. Heat Mass Transfer 39 (12) (1996) 2599–2608.

[5] W. Qu, G.M. Mala, D. Li, Pressure-driven water flows in trapezoidal silicon microchannels, Int. J. Heat Mass Transfer 43 (2000) 3925–3936.

[6] F. Debray, J.P. Franc, T. Maître, S. Reynaud, Measurement of forced convection heat transfer coefficients in mini-channels, Mec. Ind. 2 (2001) 443–454.

[7] B. Agostini, B. Watel, A. Bontemps, B. Thonon, Friction factor and heat transfer coefficient of R134a liquid flow in mini-channels, Appl. Therm. Eng. 22 (2002) 1821–1834.

[8] R. Shah, A. London, Laminar Flow Forced Convection in Ducts, Academic Press, 1978.

[9] D. Maillet, S. André, J.C. Batsale, A. Degiovanni, C. Moyne, Thermal Quadrupoles, Wiley, Chichester, 2000.

[10] G.I. Maranzana, P.D. Maillet, Quasi-analytical simulation of conduction heat transfer through a pyramidal multilayer multiblock by the quadrupole method, Numer. Heat Transfer B 42 (2002) 399–421.

[11] H. Stehfest, Remarks on algorithm368, numerical inversion of Laplace transforms, Comm. ACM 13 (1970) 624.

[12] G. Maranzana, I. Perry, D. Maillet, Modeling of conjugate heat transfer between parallel plates separated by a hydrodynamically developed laminar flow by the quadrupole method, Numer. Heat Transfer, Part A 46 (2004) 1–19.

[13] A. Bendada, D. Maillet, J.C. Batsale, A. Degiovanni, Reconstruction of a non-uniform interface thermal resistance by inverse conduction, Inverse Probl. Eng. 6 (1998) 79–123.

[14] R.B. Peterson, Numerical modelling of conduction effects in microscale counterflow heat exchangers, Microscale Thermophys. Eng. 3 (1999) 17–30.